Journal of Materials Science and Chemical Engineering, 2024, 12, 108-122
https://www.scirp.org/journal/msce
ISSN Online: 2327-6053
ISSN Print: 2327-6045

Synthesis of Low-Cost γ-Nano Alumina-Based Kaolinitic Clay: Effect of Pre-Heating Temperature of the Precursor

Gustave Tchanang[1,2*], Jean M. Kepdieu[2], Kalaya Goumou[1], Mamadou Y. Baldé[2,3], Cyprien J. Ekani[2], Chantale N. Djangang[2], Phillipe Blanchart[4]

[1]Department of Chemistry, University Julius Nyerere of Kankan, Kankan, Guinea
[2]Department of Inorganic Chemistry, University of Yaoundé I, Yaoundé, Cameroon
[3]Department of Chemistry, University Gamal Abdel Nasser of Conakry, Conakry, Guinea
[4]Institute of Research on Ceramics of Limoges, University of Limoges, Limoges, France
Email: *tchanang.gustave@yahoo.com

How to cite this paper: Tchanang, G., Kepdieu, J.M., Goumou, K., Baldé, M.Y., Ekani, C.J., Djangang, C.N. and Blanchart, P. (2024) Synthesis of Low-Cost γ-Nano Alumina-Based Kaolinitic Clay: Effect of Pre-Heating Temperature of the Precursor. *Journal of Materials Science and Chemical Engineering*, **12**, 108-122.
https://doi.org/10.4236/msce.2024.1212008

Received: November 25, 2024
Accepted: December 27, 2024
Published: December 30, 2024

Copyright © 2024 by author(s) and Scientific Research Publishing Inc.
This work is licensed under the Creative Commons Attribution International License (CC BY 4.0).
http://creativecommons.org/licenses/by/4.0/
Open Access

Abstract

Nano alumina was synthesised using precursors from pre-heated kaolinitic clay at 600˚C, 700˚C, and 800˚C following by a bottom-up sol gel method that led to $Al(OH)_3$. The latter was subsequently calcinated at 900˚C to form γ-nano alumina (γ-Al_2O_3). The final products were characterised using X-ray Diffraction (XRD), Fourier transformed infrared Spectroscopy (FTIR), Scanning electron Microscopy (SEM) coupled with Energy dispersive X-ray analysis (EDX) as well as Brunauer-Emmett-Teller (BET) for specific surface area measurement. The γ-nano alumina confirmed by X-ray patterns and infrared spectroscopy was found to be in a poorly crystalized form with 6.8 nm as crystallite size. The specific surface area and the synthesis yield varied with the temperature of pre-heating kaolinitic clay. The best process yield, 17.88%, and specific surface area of 146.78 m^2/g, was obtained with 700˚C as the best pre-heating temperature of the precursor. Due to the characteristics of the product obtained, they could be very interesting in many applications such as adsorption given their high specific area and nanoscale structure.

Keywords

Clay, Nanoparticles, Characterization, Yield Synthesis

1. Introduction

Alumina, also known as aluminum trioxide of stoechiometric formula Al_2O_3, is known as one of the most widely metal oxides used in ceramics, metallurgical, and

chemical industries due to its interesting properties such as high-temperature resistance, hardness, high melting point, thermal conductivity, amphotericity, chemical inertness, abrasion resistance, good surface properties [1] [2]. The nanoscale confers high-performance properties such as enhanced mechanical strength, greater chemical reactivity, high electrical conductivity, interesting fluorescence, etc. [3]-[5]. The improvement in physico-chemical and structural characteristics is mainly due to the significant increase in specific surface area and porosity. These exceptional properties depend essentially on particle size and distribution [6].

Alumina, well-known in its α, β, γ, η, θ, κ, and χ structural phases, is one of the most common adsorbents used in environmental engineering such as adsorption and catalysis, with remarkable optical and electronic properties [7] [8]. Several research works have also demonstrated the interesting properties of alumina nanoparticle such as stability, low toxicity, the ability to be functionalized with a range of molecules and biocompatibility, which are favourable for their use in biology [6] [9]. These properties depend essentially on the microstructure, which is inseparable from the raw materials used and the synthesis process. In general, alumina nanoparticles are synthesized from industrial precursors, including aluminum chloride, isopropoxides, and aluminum nitrates [10] [11]. The use of chemicals precursors for the synthesis is not really eco-friendly. Since nano alumina has a broad range of applications, development of low-cost processing routes for its synthesis is one of the most prominent industrial challenges [10]-[12].

Numerous processes for synthesizing alumina nanoparticles are described in the literature, including the sol-gel method [9] [13], microwave and vapor-phase, precipitation and leaching techniques, mechanochemical method, solvothermal method, and so on [12] [14]. In those different techniques, the control of the particles size, the pore distribution as well as the specific surface area remains a very interesting and challenging aspect. Alumina nanoparticle in its gamma structure (γ-Al_2O_3) has a high specific surface area and therefore more effective in afore mentioned applications [8] [13] [15]. In the perspective of sustainable development, there is a growing trend for investigations using agro-industrial waste such as red mud, fly ash or even less used mineral materials [6] [9]. Few workers have, however, used clays materials such as kaolinitic clay for the synthesis of nano alumina was nevertheless successfully obtained product with high specific area, mechanical, and thermal stability properties [16]-[18].

That's when we propose to synthesize nano alumina from kaolinitic clay with emphasis on the effect of the pre-heating temperature of the precursor and evaluate product properties (specific surface area especially) by comparison with the results of others works. The kaolinitic clay is available and constitutes an alternative precursor to chemicals reagents for the synthesis of nano alumina.

2. Experimental Methods

2.1. Materials

The Kaolinitic clay (Kc) used in this work was from Dibamba, Littoral Region of

Cameroon. Some chemicals such as sucrose pellets (99 wt%), hexane (96 wt%), hydrochloric acid (32 wt%), ammoniac (99.5 w%) acquired from PROLABO Ltd. were also used in minor quantities. The chemicals were used without any further purification.

2.2. Characterization and Procedures

The clay material was characterized by several techniques described as follow: the chemical composition was carried out by ICP analysis and the X-ray diffraction (performed with Bruker D8 Advance with Cu Kα1 radiation equipment). The differential coupled with gravimetric thermal (DTA/TGA) analyses using a Setsys 2400 de SETARAM apparatus, heating rate 5˚C/min). The phase composition was investigated by Fourier transform infrared spectra recorded in the range of 4000 - 300 cm^{-1} using Bruker FT-IR Tensor 27 spectrophotometer.

The mineralogical phase was enriched by wet sieving at 75 µm, and it was dried to obtain a powder fraction labelled as Kc. The synthesis process was in few steps, starting with the thermal activation of the clay at 600˚C, 700˚C, and 800˚C for 1 hour in a model LH60/14 muffle furnace with a heating rate of 5˚C/min to deliver precursors according with the following equation.

$$Al_2O_3\cdot 2SiO_2\cdot 2H_2O(Kc)\xrightarrow{600\text{-}800^{\circ}C}Al_2O_3\cdot 2SiO_2(\text{metakaolinite})+2H_2O \quad (1)$$

The samples obtained were labelled MK600, MK700, MK800, where MK stands for Metakaolin. Those precursors were used for the synthesis of alumina nanoparticles following a modified sol-gel associated with the bottom-up process [19] [20]. Indeed, each precursor was chemically treated with a 2.5 N solution of hydrochloric acid for 2 hours at 90˚C, (5 > pH > 3) as shown in Equation (2).

$$\begin{aligned}&Al_2O_3\cdot 2SiO_2+(Fe_2O_3,TiO_2,SiO_2)+HCl\\&\rightarrow 2SiO_2(\text{residue})+\left(n\left[Al(H_2O)\right]^{3+}+3nCl^{-}+\left[Fe^{3+}+Ti^{4+}\right]\right)(\text{aqueous filtrate})\end{aligned} \quad (2)$$

The mixture was filtered and the filtrate was then kept for further use. The amphoteric character of aluminum (III) species is preferentially shifted to basic to facilitate its solubility in the water together with other oxides. The liquid phase recovered, typically alumina was submitted to react with ammonium hydroxide (NH_4OH) to form Aluminum hydroxide ($Al(OH)_3$) which is then soaked in hexane to purify it and dried. Sucrose was added to minimize the particle agglomeration.

$$\begin{aligned}&AlCl_3(aq)+C_{11}H_{22}O_{11}(s)+3NH_4OH(l)\\&\rightarrow Al(OH)_3+3NH_4Cl(g)+10C(s)+10H_2(g)+CO_2(g)+H_2O(l)+4O_2(g)\end{aligned} \quad (3)$$

The Aluminum hydroxide ($Al(OH)_3$) obtained is then soaked in an appropriate quantity of hexane for 24 hours, then dry after filtration. The role of hexane is to rid the product of more organics impurities. The calcination at 900˚C of product in the last step permits the transformation in amorphous phase following the Equation (4).

$$Al(OH)_3 \xrightarrow{900^{\circ}C} \gamma\text{-}Al_2O_3 \quad (4)$$

The obtained powders were analysed with Scanning Electron Microscopy (SEM) using A Zeiss Ultra Plus FEG for surface morphology analysis, equipped with an Oxford detector EDX at 20 kV, which uses Aztec software for elemental analysis.

The chemical bonds in the final products were investigated by Fourier transform infrared spectra recorded in the range of 300 - 4000 cm^{-1} using Bruker FT-IR Tensor 27 spectrophotometer in addition to powder diffraction patterns which were recorded in the high angle 2 theta range (5˚ - 70˚) using a Bruker D8 Advance with Cu Kα1 radiation. The scan speed and step sizes were 0.3/min and 0.001˚ respectively.

The specific surface area was obtained by BET method, from N_2 adsorption and desorption isotherms at 77 K, obtained from a Carlo Erba Sorptomatic 1990 volumetric device, after outgassing the samples overnight at room temperature at a pressure lower than 10^{-4} Pa.

The yield of the synthesis process (Y) was calculated following the equation [14] [21].

$$Y(\%) = \frac{m_{NKi}}{m_{Ki}} \times 100 \quad (5)$$

where m_{NKi} is the mass of Al_2O_3 obtained in the final step of procedure and m_{Ki} is the initial mass of Al_2O_3 in calcined kaolinitic clay (600˚C, 700˚C, 800˚C).

For the determination of crystallite size, the X-ray patterns of the three alumina powders were considered. Some related peaks were then used to evaluate the average size (D) in the hkl direction, expressed in Å of the crystallites using Debye Scherrer equation [1] [22] [23].

$$D = \frac{K \times \lambda}{HL \times \cos\theta} \quad (6)$$

where k is apparatus correction constant, or Scherrer constant (0.89); HL the angular width at half-height lengh of the diffraction peak relative to the reticular plane (hkl) expressed in radians. $HL = 2\theta_{(L2)} - 2\theta_{(L1)}$; λ: wavelength of the KαCu = 1.5406 Å = 0.15406 nm; θ: half the wave deviation (half the Bragg angle, at the peak of the reflection under consideration, expressed in degrees).

3. Results and Discussion

3.1. Characteristics of the Starting Clay Material (Kc)

The chemical composition of clay material (Kc) obtained by ICP analysis was shown in **Table 1**.

The clay material has a high mass proportion of silica: SiO_2 (76.06%), while alumina is comparatively low: Al_2O_3 (14.65%). This gives a SiO_2/Al_2O_3 molar ratio of 5.19, classifying the clay as siliceous [24] [25]. In general, alkaline oxides (Na_2O, K_2O) and alkaline earth oxides (CaO, MgO) were present in very small quantities.

This indicates that the material is a low-melting point [4] [26]. The coloring oxides TiO_2 and Fe_2O_3 are present in very small quantities.

Figure 1 shows the (XRD) patterns of the clay material (Kc). Some peaks of crystalline phases were revealed.

Table 1. Chemical composition of raw clay material.

Oxides	SiO_2	Al_2O_3	Fe_2O_3	MgO	MnO	CaO	Na_2O	K_2O	TiO_2	P_2O_5	LF[#b]
W (%)	76.06	14.65	2.04	0.10	-	0.07	-	0.11	DL[#a]	-	8.04

a. detection Limit; b. loss on fire.

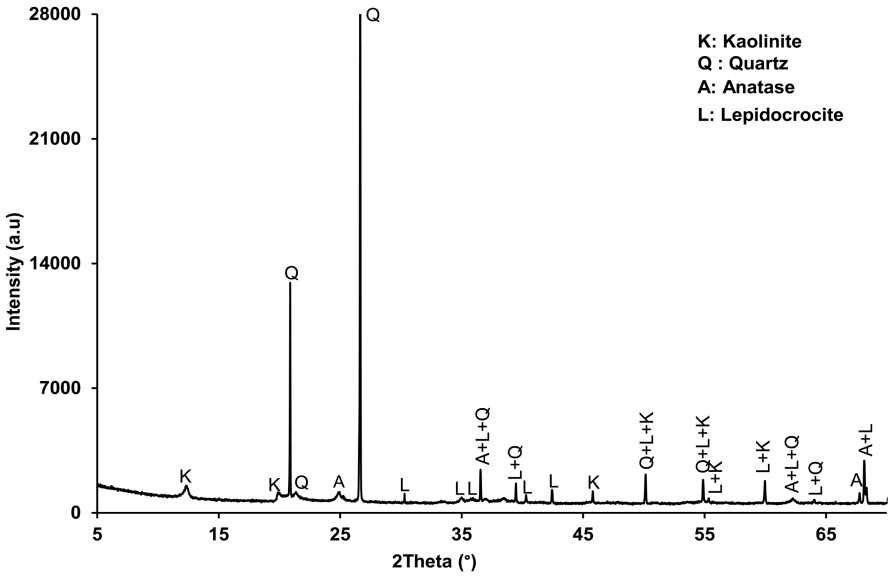

Figure 1. X-ray patterns of clay material, (K) Kaolinite, (Q) Quartz), (A) Anatase, (L) Lepidocrocite.

Kaolinite ($Al_2Si_2O_5(OH)_4$) (JCPDS 14-164) is the main mineral phase of the clay material studied, associated with other phases as quartz (JCPDS 5-490) (SiO_2), lepidocrocite (FeOOH) (JCPDS 8-98), and anatase (TiO_2) (JCPDS 4-447).

The infrared spectrum of Kc presented in Figure 2 showed the typical appearance of a kaolinite spectrum [3] [27]. The absorption bands at 3440 and 3370 cm^{-1} corresponds to the vibrations of the O-H bonds of the adsorbed water molecules, while those at 3689, 3647, and 3619 cm^{-1} are attributed to the symmetrical elongation vibrations of the free OH groups on the external surface and the elongation vibrations of the internal -OH groups of the kaolinite [14] [27]. The absence of the absorption band between 3665 and 3670 cm^{-1} reflects an inversion of the band intensities at 3647 and 3670 cm^{-1}. This is only observed when there is disorder within the material [25] [26] [28]. The absorption bands located around 1114 - 1116 cm^{-1}, 998-1025 cm^{-1} on the spectrum correspond respectively to the deformation vibrations of the Si-O and symmetrical Si-O-Si and asymmetrical Si-O-Al bonds [25] [29], while the bands at 908 and 909 cm^{-1} as well as those at 788 - 792

cm^{-1}, 747 cm^{-1} and 663-677 cm^{-1} were attributed to the vibrations of the Al-O-Si and Al-OH bonds in kaolinite. The shoulders around 521 - 523 cm^{-1}, and 458 cm^{-1} shows the deformation vibrations of the Si-O-Si and Si-O-Al bonds [30] [31]. Shoulders around 1150, 714, and 695 cm^{-1} indicated the presence of quartz [25].

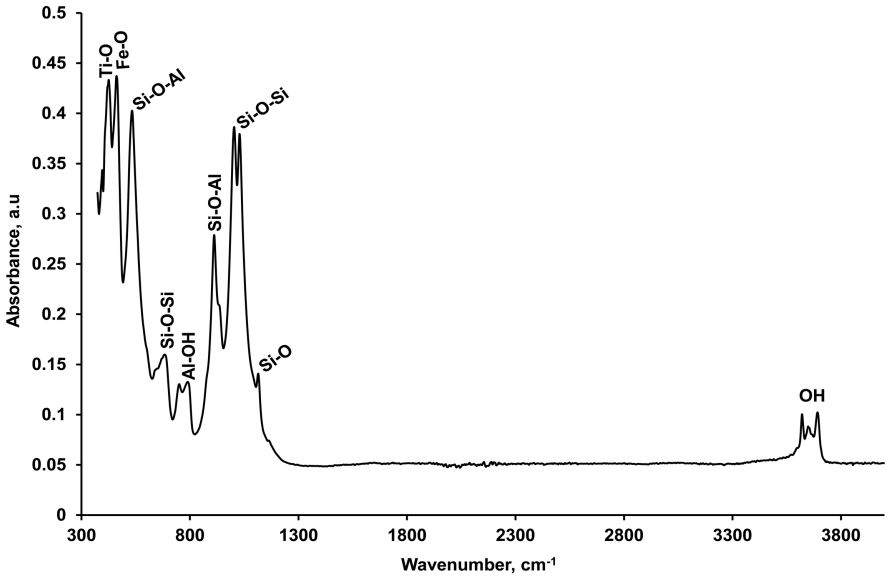

Figure 2. Fourier transform infrared spectra of clay.

Figure 3 showed the (DTA and TGA) thermograms of the clay material and revealed that the shapes of the two curves were typical to those of kaolinitic clays [16] [26] [28] [32].

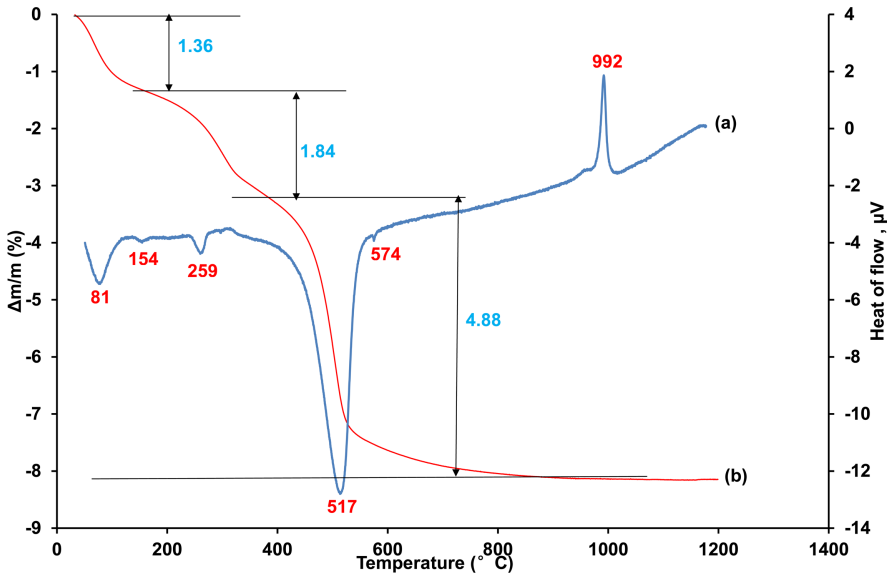

Figure 3. Plots of (a) DTA and (b) TGA thermograms of clay material (Kc).

An endothermic peak on the DTA thermogram of clay around 80˚C accompanied by a small loss of mass on the (TGA) curve, this thermal incident would

correspond to the endothermic phenomenon of the departure of the water of hydration molecules [32] [33]. An endothermic peak was observed around 260˚C, with a mass loss of around 1.84% on the (TGA) curve corresponding to the dehydroxylation of lepidocrocite (γ-FeO(OH)) into maghemite (γ-Fe_2O_3) according the equation [25] [28].

$$\underset{\text{Lepidocrocite}}{2\gamma\text{-FeOOH}} \xrightarrow{259^{\circ}\text{C}} \underset{\text{Maghemite}}{\gamma\text{-}Fe_2O_3} + \underset{\text{Water}}{H_2O} \tag{7}$$

The content of this mineral from the proportion of loss on ignition related to this mineral gives 10.18% Lepidocrocite. Another endothermic phenomenon occurs between 400˚C and 600˚C, corresponding to the dehydroxylation of kaolinite to form metakaolinite [25] [32].

$$\underset{\text{Kaolinite}}{Si_2O_5Al_2(OH)_4} \xrightarrow{500^{\circ}\text{C}} \underset{\text{Metakaolinite}}{2SiO_2 \cdot Al_2O_3} + \underset{\text{water of constitution}}{2H_2O} \tag{8}$$

Around 574˚C there is an endothermic phenomenon with no loss of mass that reflects the polymorphic transformation of alpha quartz into béta quartz as shown in following equation.

$$\underset{\text{quartz } \alpha}{\alpha\text{-}SiO_2} \xrightarrow{573^{\circ}\text{C}} \underset{\text{quartz } \beta}{\beta\text{-}SiO_2} \tag{9}$$

Between 900˚C and 1000˚C, the exothermic peak on the DTA curves corresponds to the reorganization of metakaolinite and the formation of pseudo-spinel [34].

$$\underset{\text{Metakaolinite}}{2(2SiO_2 \cdot Al_2O_3)} \xrightarrow{925\text{-}1000^{\circ}\text{C}} \underset{\text{Pseudo-spinelle}}{2Al_2O_3 \cdot 3SiO_2} + \underset{\text{crystalized Silica}}{SiO_2} \tag{10}$$

These observations confirm that the treatment of Kaolinitic clay (Kc) up to 700˚C, transformed it into metakaolinite which is a more reactive amorphized form. At this temperature, no reorganized phase was yet detected, which proves that the whole system was indeed activated so that hydrated minerals can decompose into primitive oxides [25] [32].

3.2. Characteristics of the Synthesized Alumina Nanoparticles

3.2.1. XRD Patterns

The X-ray patterns (**Figure 4**) of the three products synthesized on the basis of precursors MK600, MK700, and MK800 respectively permitted the determination of the mineralogical phases. The three diffractograms exhibit peaks which characterize γ-nano alumina (2θ = 37.15; 46.15, and 66.75˚). These peaks correspond respectively to the (311), (400), and (440) planes on JCPDS file No. 29-63 [14] [35] [36]. The phases were therefore in a very poorly crystallized state given the amount of amorphous phase. The areas under the peaks were of similar sizes and do not really depend on the pre-heating temperature of the precursor. This can be explained by the further changes due to chemical reaction during the synthesis process. The so-called amorphous phase may be linked to the residual organic matter.

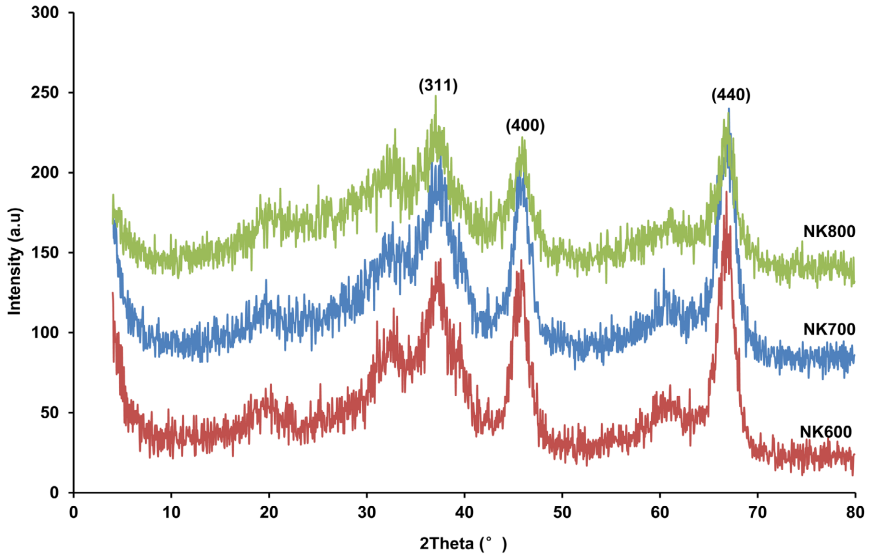

Figure 4. XRD patterns of nanolumina NK600 (from MK600), NK700 (from MK700), and NK800 (from MK700).

3.2.2. Crystallite Size

The zoom of hkl (440) peak has been assumed to be representative due to its highest intensity and used in the calculation of crystallite size (**Figure 5**).

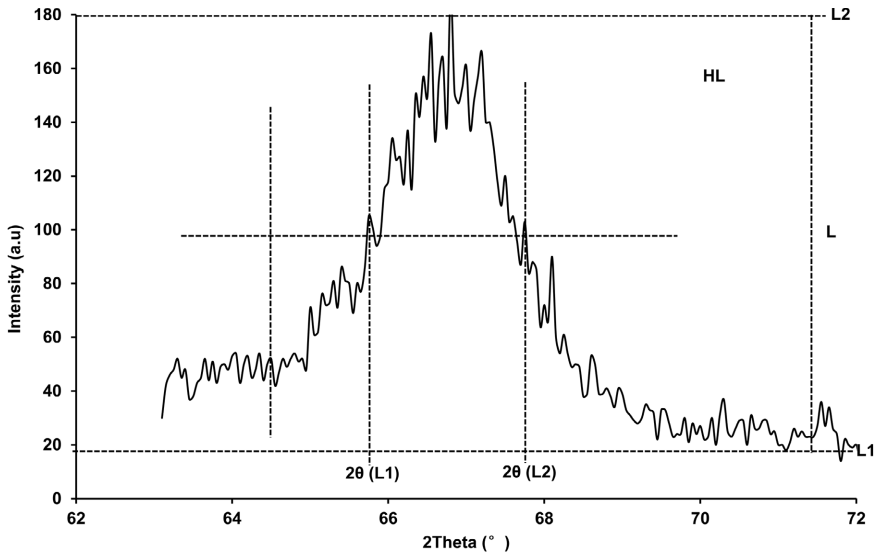

Figure 5. Peak of plane (440) to the nano alumina diffractogram.

Table 2 shows the different values of the calculation parameters used to calculate the crystallite size Equation (6).

Table 2. Parameters of the calculations of the crystallite size.

Parameters	2θ (L1)	2θ (L2)	$\Delta(2\theta)^\circ$	$\Delta(2\theta)$ r	θ	Cos (θ)	D/nm
NKi	65.55	67.85	2.30	0.040	0.020	0.99	6.81

3.2.3. FTIR of Nano Alumina

The (FTIR) spectra (**Figure 6**) of the three synthesized products (NK600, NK700, and NK800) showed that the spectra were all similar and display characteristic adsorption bands of nano alumina [14] [15] [35]. Around 450 and at 1090 cm^{-1} are the stretching vibration bands of the Al-O-Al bond. Around 1646 cm^{-1} was located a peak related to the bending mode of physically adsorbed water molecules. At around 3358 cm^{-1} were the stretching vibrations of bonded OH groups and isolated OH groups [8] [14] [35]. Despite the difference in the pre-heating temperature, the bands are similar showing that the bonds present in the three synthesized products are the same.

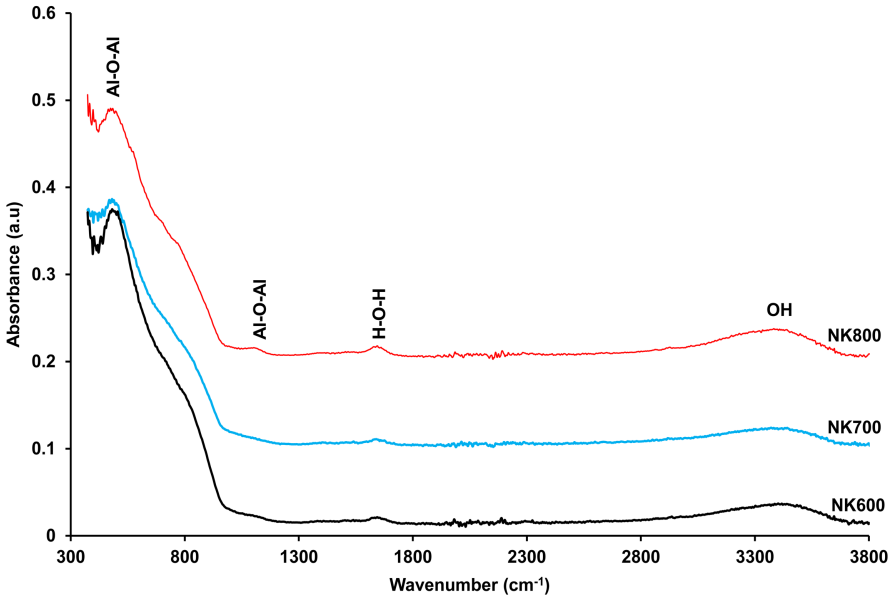

Figure 6. FTIR spectra of NK600, NK700, and NK800.

3.2.4. SEM/EDX of Nano Alumina

The SEM images of the alumina nanoparticles from precursor previously heated at 600˚C, 700˚C, and 800˚C presented in **Figure 7** revealed that all the products have heterogeneous morphology, with large particles dominating in the case of NK600 and NK700, compared with NK800, where the particles were less large and closer. Moreover, the particles seem to be isolated from each other, independently of their respective sizes. These images were similar to those of alumina nanoparticles found by some authors using different precursors [3] [8] [27]. In addition, EDX analysis of the contrasts in each of the products clearly shows that the species present in high proportion are aluminum (Al) and oxygen (O). This suggests that the chemical substance present was aluminum oxide (Al_2O_3).

3.2.5. Specific Surface Area of Nano Alumina

According to the surface morphology analysis, the specific surface area (SSA) of NK600, NK700, and NK800 were 141.7, 146.8, and 137.7 m^2/g for precursor pretreated at 600˚C, 700˚C, 800˚C respectively. The more reactivity of the precursor,

higher the SSA of the nano alumina obtained was observed. Furthermore, the values were challenging with those found in the literature [3] [8] [12].

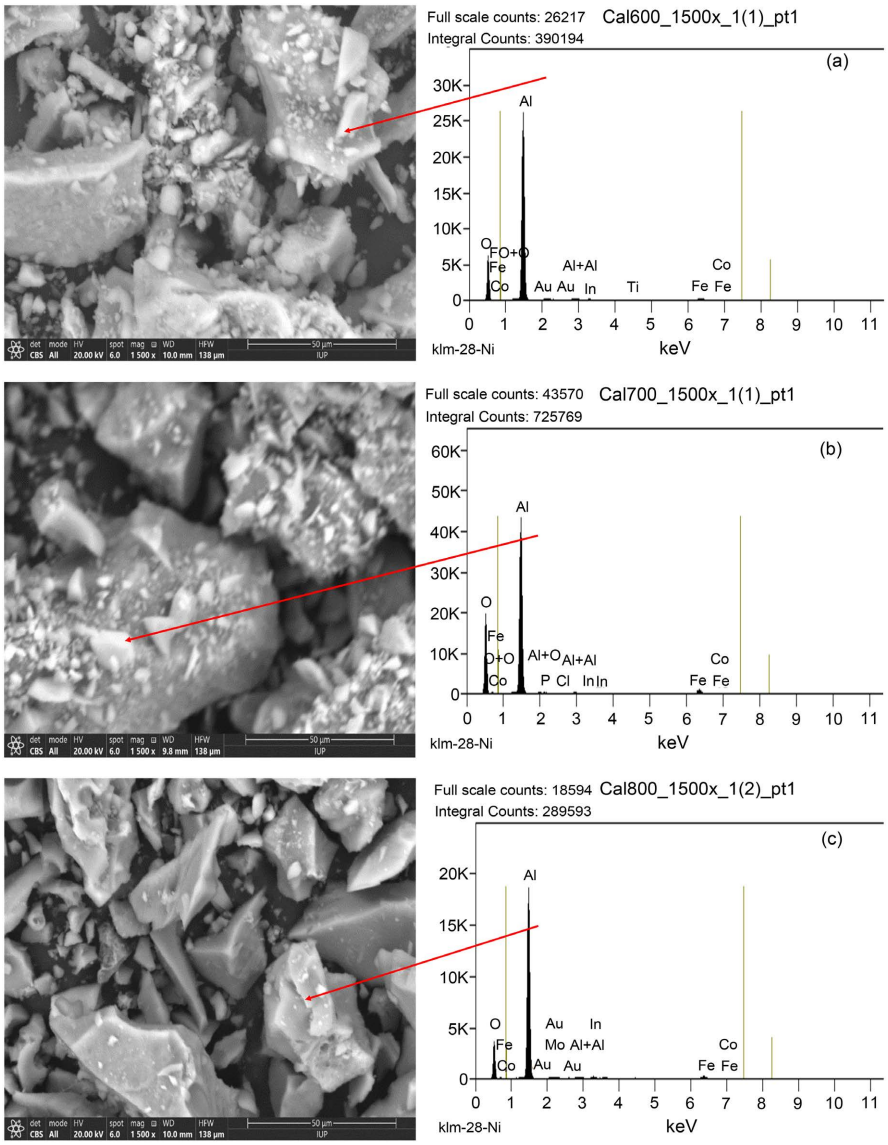

Figure 7. SEM images and EDX analysis of Nano alumina (a) NK600, (b) NK700, (c) NK800.

3.3. Synthesis Process Yield

Table 3 gives the synthesis yield from the three precursors. The synthesis yield, calculated through Equation (5) and presented in Table 3, was found to be 17.88 % for the amorphization temperature of 700˚C compared with 14.4% and 12.24 obtained at 600˚C and 800˚C respectively. These values were well below those given by industrial precursors [14] [34] [35]. The results were in accordance with the respective reactivity of the precursors. Indeed, at the lower of 600˚C the clay material was not completely amorphized and the bonds between the tetrahedral and octahedral planes of the clay sheets were not sufficiently weakened to optimize oxide dissolution during

acid leaching and promote good synthesis yield. One part of the chemicals (HCl and NH_4OH) might be used to dissolve the network.

Table 3. Synthesis yield of nano alumina particle.

Precursors	MK600	MK600	MK600
Yield (%)	14.4	17.88	12.24

The precursor obtained at 700˚C (MK700) was the most reactive due to the transformation of the clay material into primitive oxides [25] [32]. In fact, as amorphization was linked to dehydroxylation, it has been shown by some authors that residual hydroxyl groups, around 10% of the -OH present in metakaolinite after its formation, were gradually eliminated [16] [35]. In addition, infrared studies of kaolinite dehydroxylation kinetics have shown that it was the -OH of the less firmly bonded outer octahedral sheets that first react with each other, releasing around three-quarters of the water of constitution, followed by the elimination of the better-protected -OH of the tetrahedral and octahedral sheets. Whereas at 800˚C, the reorganization process has already begun, involving the alumina species, since some authors believe that the reorganization observed on the (TGA/DTA) thermogram has a combined effect resulting on the one hand, from the demixing of the system into Al_2O_3 rich domains and, on the other, from the diffusion of small, anisotropic particles at the grain boundary interfaces [20] [35].

The metakaolinite in MK800 tends to give rise to a pseudo-spinel phase and the amorphous silica to a more crystalized form of quartz, or cristobalite. This leads to a more organized structure that finally decreases the reactivity of the precursor subsequently to useless consumption of reactants. Based on these results, the optimum temperature for amorphization of the material is 700˚C.

A comparison of the present nano alumina particles with other obtained from different precursors has been made and the results are presented in **Table 4**.

Table 4. Comparison of SSA and crystallite size with other works.

Precursors	Specific surface area (m^2/g)	Crystallite size (nm)	Related references
Aluminum dross (Calcium aluminum oxide)	36.46	75	[3]
Aluminum nitrate: $Al(NO_3)_3{\cdot}9H_2O$	76	63.4	[35]
Aluminum chlorite: $AlCl_3{\cdot}6H_2O$	112.9	4.13	[8]
Alumina nanoparticle with SDS modification	221.3	40	[37]
Nano alumina from MK700	146.8	6.8	Present work

According to **Table 4** above, the nano alumina synthesized in this work exhibits a higher SSA compared with many other adsorbents obtained from chemicals reagents and this is in accordance with the smaller crystallite size. Also, it

might be of great economic interest since it was obtained from low-cost available materials. Such good properties may broaden the applications fields of the product.

4. Conclusion

The aim of the present study was to investigate the effect of pre-heating temperature of the precursors (kaolinitic clay) for the synthesis of alumina nanoparticles. The kaolinitic clay was pre-treated at different temperatures 600˚C, 700˚C, and 800˚C to obtain more reactive precursors. The latter underwent chemical reactions subsequently with Chlorhydric acid and Ammonium hydroxide solutions followed by further treatment in sucrose and hexane. Three nano alumina NK600, NK700, and NK800 were successfully obtained and characterized by (XRD, FTIR spectroscopy, SEM/EDX), (BET) surface specific surface area. The yield of these particles varied with the amorphization temperature of the starting clay: 14.4% at 600˚C, 17.88% at 700˚C, and 12.24% at 800˚C. The X-ray patterns and infrared spectroscopy indicated that γ-nano alumina was effectively obtained with crystallite size around 6.8 nm. The (BET) specific surface area (SSA) of NK600, NK700, and NK800 were 141.7; 146.8, and 137.7 m^2/g for precursor pre-treated at 600˚C, 700˚C, 800˚C respectively. Scanning electron microscopy showed that the particles had a tendency to be isolated from each other, creating more active surface and porosity and thus promoting great reactivity. These results show that heat treatment of the initial material is important, increasing the characteristics of the final product. In this work, 700˚C is the optimum temperature for heat treatment of the initial material (good yield, small crystallite size, high specific surface area).

Informed Consent Statement

All the authors are voluntarily participating for the submission of this research work.

Consent to Publication

The authors confirm that this manuscript has not been submitted or published previously to any other journal and give full consent for publication of the research work.

Data Availability

The datasets generated during and/or analyzed during the current study are available from the corresponding author on reasonable request.

Authors Contributions

Gustave Tchanang & Jean Marie Kepdieu: Investigation, Roles/Writing—original draft, Data curation. Njiomou Djangang Chantale: Conceptualization, Methodology;

Writing—review & editing, Visualization. Cyprien Joel Ekani: Investigation, Writing—review & editing. Mamadou Yaya Baldé, Kalaya Goumou and Phillipe blanchard: Methodology, Writing—review & editing.

Conflicts of Interest

All authors certify that they have no affiliations with or involvement in any organization or entity with any financial interest or non-financial interest in the subject matter discussed in this manuscript.

References

[1] Alqahtani, W.M.S., Abdul, N.S., Aslam, K., Alanazi, A., Ansary, N., Alresayes, S.S., *et al.* (2023) PEEK Surface Treatment on Surface Roughness and Bond Integrity to Composite Resin Utilizing Er: YAG, Rosebengal Activated by PDT, and Aluminum Trioxide Particles. *Photodiagnosis and Photodynamic Therapy*, **44**, Article ID: 103879. https://doi.org/10.1016/j.pdpdt.2023.103879

[2] Yadav, A.K. and Bhattacharyya, S. (2019) Preparation of Porous Alumina Adsorbent from Kaolin Using Acid Leach Method: Studies on Removal of Fluoride Toxic Ions from an Aqueous System. *Adsorption*, **26**, 1073-1082. https://doi.org/10.1007/s10450-019-00193-4

[3] Breky, M.M.E., Borai, E.H. and Kassem, A.T. (2019) Synthesis of High-Grade Alumina from Aluminium Dross and Its Utilization for the Sorption of Radioactive Cobalt. *Desalination and Water Treatment*, **170**, 265-276. https://doi.org/10.5004/dwt.2019.24732

[4] Gonidanga, B.S., Njoya, D., Lecomte-Nana, G. and Njopwouo, D. (2019) Phase Transformation, Technological Properties and Microstructure of Fired Products Based on Clay-Dolomite Mixtures. *Journal of Materials Science and Chemical Engineering*, **7**, 1-14. https://doi.org/10.4236/msce.2019.711001

[5] Teles, F., Martins, G. and Antunes, F. (2022) Fire Retardancy in Nanocomposites by Using Nanomaterial Additives. *Journal of Analytical and Applied Pyrolysis*, **163**, Article ID: 105466. https://doi.org/10.1016/j.jaap.2022.105466

[6] Aghapour, F., Moghadamnia, A.A., Nicolini, A., Kani, S.N.M., Barari, L., Morakabati, P., *et al.* (2018) Quercetin Conjugated with Silica Nanoparticles Inhibits Tumor Growth in MCF-7 Breast Cancer Cell Lines. *Biochemical and Biophysical Research Communications*, **500**, 860-865. https://doi.org/10.1016/j.bbrc.2018.04.174

[7] Adesina, A.O., Elvis, O.A., Mohallem, N.D.S. and Olusegun, S.J. (2019) Adsorption of Methylene Blue and Congo Red from Aqueous Solution Using Synthesized Alumina-Zirconia Composite. *Environmental Technology*, **42**, 1061-1070. https://doi.org/10.1080/09593330.2019.1652696

[8] Ali, S., Abbas, Y., Zuhra, Z. and Butler, I.S. (2019) Synthesis of γ-Alumina (Al_2O_3) Nanoparticles and Their Potential for Use as an Adsorbent in the Removal of Methylene Blue Dye from Industrial Wastewater. *Nanoscale Advances*, **1**, 213-218. https://doi.org/10.1039/c8na00014j

[9] Sdiri, A., Higashi, T., Bouaziz, S. and Benzina, M. (2014) Synthesis and Characterization of Silica Gel from Siliceous Sands of Southern Tunisia. *Arabian Journal of Chemistry*, **7**, 486-493. https://doi.org/10.1016/j.arabjc.2010.11.007

[10] Potdar, H.S., Jun, K., Bae, J.W., Kim, S. and Lee, Y. (2007) Synthesis of Nano-Sized Porous γ-Alumina Powder via a Precipitation/digestion Route. *Applied Catalysis A*:

General, **321**, 109-116. https://doi.org/10.1016/j.apcata.2007.01.055

[11] Behera, P.S., Sarkar, R. and Bhattacharyya, S. (2016) Nano Alumina: A Review of the Powder Synthesis Method. *Interceram—International Ceramic Review*, **65**, 10-16. https://doi.org/10.1007/bf03401148

[12] Ghanizadeh, S., Bao, X., Vaidhyanathan, B. and Binner, J. (2014) Synthesis of Nano *α*-Alumina Powders Using Hydrothermal and Precipitation Routes: A Comparative Study. *Ceramics International*, **40**, 1311-1319. https://doi.org/10.1016/j.ceramint.2013.07.011

[13] Shojaie-Bahaabad, M. and Taheri-Nassaj, E. (2008) Economical Synthesis of Nano Alumina Powder Using an Aqueous Sol-Gel Method. *Materials Letters*, **62**, 3364-3366. https://doi.org/10.1016/j.matlet.2008.03.012

[14] Tantawy, M.A. and Ali Alomari, A. (2019) Extraction of Alumina from Nawan Kaolin by Acid Leaching. *Oriental Journal of Chemistry*, **35**, 1013-1021. https://doi.org/10.13005/ojc/350313

[15] Nikoofar, K., Shahedi, Y. and Chenarboo, F.J. (2019) Nano Alumina Catalytic Applications in Organic Transformations. *Mini-Reviews in Organic Chemistry*, **16**, 102-110. https://doi.org/10.2174/1570193x15666180529122805

[16] Baba, A.A., Raji, M.A., Muhammed, M.O., Abdulkareem, A.Y., Olasinde, F.T., Ayinla, K.I., *et al.* (2019) Potential of a Nigerian Biotite-Rich Kaolinite Ore to Industrial Alumina by Hydrometallurgical Process. *Metallurgical Research & Technology*, **116**, Article No. 222. https://doi.org/10.1051/metal/2018076

[17] Said, S., Mikhail, S. and Riad, M. (2020) Recent Processes for the Production of Alumina Nano-Particles. *Materials Science for Energy Technologies*, **3**, 344-363. https://doi.org/10.1016/j.mset.2020.02.001

[18] Zulfiqar, U., Subhani, T. and Husain, S.W. (2016) Synthesis and Characterization of Silica Nanoparticles from Clay. *Journal of Asian Ceramic Societies*, **4**, 91-96. https://doi.org/10.1016/j.jascer.2015.12.001

[19] Fatimah, I., Sumarlan, I. and Alawiyah, T. (2015) Fe(III)/TIO_2-Montmorillonite Photocatalyst in Photo-Fenton-Like Degradation of Methylene Blue. *International Journal of Chemical Engineering*, **2015**, Article ID: 485463. https://doi.org/10.1155/2015/485463

[20] Kumar, D., Wu, X., Fu, Q., Ho, J.W.C., Kanhere, P.D., Li, L., *et al.* (2015) Hydrophobic Sol-Gel Coatings Based on Polydimethylsiloxane for Self-Cleaning Applications. *Materials & Design*, **86**, 855-862. https://doi.org/10.1016/j.matdes.2015.07.174

[21] Tchanang, G., Djangang, C.N., Abi, C.F., Moukouri, D.L.M. and Blanchart, P. (2021) Synthesis of Reactive Silica from Kaolinitic Clay: Effect of Process Parameters. *Applied Clay Science*, **207**, Article ID: 106087. https://doi.org/10.1016/j.clay.2021.106087

[22] Kipling, J.J. and Wilson, R.B. (1960) Adsorption of Methylene Blue in the Determination of Surface Areas. *Journal of Applied Chemistry*, **10**, 109-113. https://doi.org/10.1002/jctb.5010100303

[23] Li, X., Ou, Y., Li, C., Zhu, J. and Zhi, P. (2019) Preparation of Alumina from Aluminum Ash by Sintering with Sodium Hydroxide. *IOP Conference Series*: *Earth and Environmental Science*, **233**, Article ID: 042027. https://doi.org/10.1088/1755-1315/233/4/042027

[24] Njiomou Djangang, C., Lecomte, G.L., Soro, J., Elimbi, A., Blanchart, P. and Njopwouo, D. (2010) Elaboration de céramiques poreuses à base de sciure de bois et de deux argiles du Cameroun. *Annales de chimie Science des Matériaux*, **35**, 1-16. https://doi.org/10.3166/acsm.35.1-16

[25] Kakali, G., Perraki, T., Tsivilis, S. and Badogiannis, E. (2001) Thermal Treatment of Kaolin: The Effect of Mineralogy on the Pozzolanic Activity. *Applied Clay Science*, **20**, 73-80. https://doi.org/10.1016/s0169-1317(01)00040-0

[26] Mazghouni, M., Kbir-Ariguib, N., Counioux, J.J. and Sebaoun, A. (1981) Etude Des Equilibres Solide—Liquide—Vapeur Des Systemes Binaires K_3PO_4 H_2O Et $Mg_3(PO)_2$ H_2O. *Thermochimica Acta*, **47**, 125-139. https://doi.org/10.1016/0040-6031(81)85099-x

[27] Salahudeen, N., Ahmed, A.S., Al-Muhtaseb, A.H., Dauda, M., Waziri, S.M. and Jibril, B.Y. (2015) Synthesis of Gamma Alumina from Kankara Kaolin Using a Novel Technique. *Applied Clay Science*, **105**, 170-177. https://doi.org/10.1016/j.clay.2014.11.041

[28] Bich, C., Ambroise, J. and Péra, J. (2009) Influence of Degree of Dehydroxylation on the Pozzolanic Activity of Metakaolin. *Applied Clay Science*, **44**, 194-200. https://doi.org/10.1016/j.clay.2009.01.014

[29] Moutou, J.M., Foutou, P.M., Matini, L., Samba, V.B., Mpissi, Z.F.D. and Loubaki, R. (2018) Characterization and Evaluation of the Potential Uses of Mouyondzi Clay. *Journal of Minerals and Materials Characterization and Engineering*, **6**, 119-138. https://doi.org/10.4236/jmmce.2018.61010

[30] Qtaitat, M.A. and Al-Trawneh, I.N. (2005) Characterization of Kaolinite of the Baten El-Ghoul Region/south Jordan by Infrared Spectroscopy. *Spectrochimica Acta Part A*: *Molecular and Biomolecular Spectroscopy*, **61**, 1519-1523. https://doi.org/10.1016/j.saa.2004.11.008

[31] Vizcayno, C., de Gutiérrez, R.M., Castello, R., Rodriguez, E. and Guerrero, C.E. (2010) Pozzolan Obtained by Mechanochemical and Thermal Treatments of Kaolin. *Applied Clay Science*, **49**, 405-413. https://doi.org/10.1016/j.clay.2009.09.008

[32] Salvador, S. (1995) Pozzolanic Properties of Flash-Calcined Kaolinite: A Comparative Study with Soak-Calcined Products. *Cement and Concrete Research*, **25**, 102-112. https://doi.org/10.1016/0008-8846(94)00118-i

[33] Autef, A., Joussein, E., Gasgnier, G. and Rossignol, S. (2012) Role of the Silica Source on the Geopolymerization Rate. *Journal of Non-Crystalline Solids*, **358**, 2886-2893. https://doi.org/10.1016/j.jnoncrysol.2012.07.015

[34] Parida, K.M., Pradhan, A.C., Das, J. and Sahu, N. (2009) Synthesis and Characterization of Nano-Sized Porous Gamma-Alumina by Control Precipitation Method. *Materials Chemistry and Physics*, **113**, 244-248. https://doi.org/10.1016/j.matchemphys.2008.07.076

[35] Banerjee, S., Gautam, R.K., Jaiswal, A., Chandra Chattopadhyaya, M. and Chandra Sharma, Y. (2015) Rapid Scavenging of Methylene Blue Dye from a Liquid Phase by Adsorption on Alumina Nanoparticles. *RSC Advances*, **5**, 14425-14440. https://doi.org/10.1039/c4ra12235f

[36] Rahmanpour, O., Shariati, A. and Nikou, M.R.K. (2012) New Method for Synthesis Nano Size γ-Al_2O_3 Catalyst for Dehydration of Methanol to Dimethyl Ether. *International Journal of Chemical Engineering and Applications*, **3**, 125-128. https://doi.org/10.7763/ijcea.2012.v3.172

[37] Chu, T.P.M., Nguyen, N.T., Vu, T.L., Dao, T.H., Dinh, L.C., Nguyen, H.L., *et al.* (2019) Synthesis, Characterization, and Modification of Alumina Nanoparticles for Cationic Dye Removal. *Materials*, **12**, Article 450. https://doi.org/10.3390/ma12030450